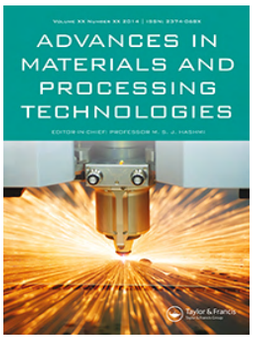

Advances in Materials and Processing Technologies

ISSN: (Print) (Online) Journal homepage: https://www.tandfonline.com/loi/tmpt20

Influence on dynamic behaviour of single layer graphene by Stone wales and pinhole defects

Manisha Makwana, Ajay M Patel, Ankit D. Oza, Manoj Kumar, Abhishek Kumar & Abhishek Joshi

To cite this article: Manisha Makwana, Ajay M Patel, Ankit D. Oza, Manoj Kumar, Abhishek Kumar & Abhishek Joshi (2023): Influence on dynamic behaviour of single layer graphene by Stone wales and pinhole defects, Advances in Materials and Processing Technologies, DOI: 10.1080/2374068X.2023.2192126

To link to this article: https://doi.org/10.1080/2374068X.2023.2192126

Published online: 19 Mar 2023.

ADVANCES IN MATERIALS AND PROCESSING TECHNOLOGIES
https://doi.org/10.1080/2374068X.2023.2192126

Influence on dynamic behaviour of single layer graphene by Stone wales and pinhole defects

Manisha Makwana[a], Ajay M Patel[b], Ankit D. Oza[c], Manoj Kumar[d], Abhishek Kumar[e] and Abhishek Joshi[f]

[a]Department of Mechanical Engineering, A D Patel Institute of Technology, Gujarat, India; [b]Mechatronics Engineering Department, G.H. Patel College of Engineering & Technology Vallabh Vidyanagar, Gujarat, India; [c]Department of Computer Sciences and Engineering, Institute of Advanced Research, Gandhinagar, Gujarat, India; [d]Department of Mechanical Engineering, ABES Engineering College, Ghaziabad, India; [e]Department of Mechanical Engineering, Pandit Deendayal Energy University, Gandhinagar, India; [f]Division of Research & Innovation, Uttaranchal University, Dehradun, India

ABSTRACT

This paper presents a computational procedure for the determination of the dynamic behaviour of graphene with different types of defects. The lattice of graphene is modelled using the molecular structural mechanics (MSM) approach, where the C–C covalent bonds are replaced by equivalent beam elements. Cantilever and bridged boundary conditions are applied for the analysis. Four types of Stone–Wales (SW) defects such as S-W (555-8), S-W (555-888-3), S-W (555-77-8) and S-W (888-3), and two types of pinhole defects with 6 and 24 elements eliminated are examined on armchair, zigzag and chiral type of graphene sheet. The effect of the structural length of the sheet, chirality and defect type on the vibrational properties of graphene sheets is investigated. The computed results reveal that SW defects produce a high frequency to that of pristine graphene, whereas the effect of pinhole defects is significant as compared to SW defects. The computed results will be useful in nano-resonator-based sensor applications.

ARTICLE HISTORY
Accepted 1 February 2023

KEYWORDS
SLG; pinhole; Stone–Wales; frequency

1. Introduction

The field of nanotechnology focuses on the study and analysis of nanostructured materials [1]. The single-layer graphene (SLG) sheet has been taken because of its extraordinary properties, such as a Young's modulus of typically 1 TPa [2]. The scientists were able to make 2D graphene, which is only one atom thick and remarkably resembles a honeycomb structure, using ordinary sticky tape. In 2D nanomaterials, Stone–Wales (SW), vacancy, pinhole, dislocation and grain boundaries defects have been identified [3]. Some defects are found during mechanical exfoliation, chemical vapour deposition and other processes. The rotation of a C–C covalent bond by 90° with respect to centre of the sheet results in the SW defect. SW defects are produced by slanted bond rotation at 90° and straight bond rotation in the horizontal and vertical directions [4,5]. These defects may be inherent in the nanomaterial

CONTACT Ankit D. Oza ankit.oza@iar.ac.in Department of Computer Sciences and Engineering, Institute of Advanced Research, Gandhinagar, Gujarat 382426, India

naturally or may be purposely incorporated into it. Additionally, during graphene self-healing, nanoparticles are formed. The effect of these kinds of defects on electrical and thermomechanical properties is a significant area of research in the field of nanofillers [6,7].

1.1. Structural defects

The effects of structural problems in graphene nanoparticles brought very little attention in the literature. The extraordinary features of graphene were anticipated by theory and proved in real-world applications. Since perfect materials are difficult to achieve, it is important to understand how they are produced and how they affect various materials, especially since they can even be purposely induced to become desirable and suitable for new solutions [8]. Intentionally implanted defects that change the properties of the material take different forms. In the 2D honeycomb structure of graphene, carbon atoms can reconfigure and restructure hexagonal lattices to produce hexagonal carbon rings [9]. The graphene fabrication methods have a significant impact on the defects [10]. The properties of the lattice structure change due to the presence of defects. The defects change the electrical structure and chemical reaction sensitivity, which changes the chemical reactivity of graphene [11].

The SW defect is a crystallographic defect that involves the change of connectivity of two σ-bonded carbon atoms, leading to their rotation by 90° with respect to the midpoint of their bond. Rotating the two planes results in the SW defect. The defects on plane of hexagonal lattice structure of SLG are shown in Figure 1. The formation of the SW defects does not result by addition or removal of carbon atoms or dangling bonds. The second is the pinhole defect. The pinhole defects are characterised by the number of absent atoms from the lattice of graphene. The finite element (FE) model of a defective graphene sheet is constructed using 2D Bernoulli beams with properties obtained from the molecular structural mechanics (MSM). The defects are uniformly distributed at the centre of the lattice structure of SLG. Dual vacancies are a common graphene symmetry reconfiguration that produces three pentagons and one octagon (555-8) but has no impact on the atomic network (Figure 1(a)). The absence of carbon atoms causes another defect in the lattice structure (555-888-3) (Figure 1(b)). One bond result in the defects (888-3) and (555-77-8) as shown in Figure 1(c,d), respectively. Pinhole defects are caused by 6 missing carbon atoms and 26 missing carbon atoms as shown in (Figure 1(e,f)). When there are more than two missing atoms, the number of possible defect configurations increases [12,13]. Other defects changes both the overall atomic weight of the crystal and the charge of the graphene. While intentionally introducing them makes charge transport more compliant, it decreases charge mobility. These impurities are introduced into the carbon lattice by replacing or functionalising specific original carbon atoms [14]. All structural issues affect physical and chemical properties, even at low concentrations. Pure graphene has a strong anisotropic charge transfer and is chemically inert. It is a safe and biocompatible biomaterial that can be used in several biological systems, but it is not suitable for many electronic applications [15]. SLG's vibrational characteristics were modelled using solid parts, spring elements and connected masses in Zg [16]. Additionally, resonance frequencies with deviations from the axis, including cantilever and bridged boundary conditions, are analysed [17–19]. In this article, the authors created SLG sheet with various chirality and lengths. Vibration analysis was done, and it revealed the frequency variations of SLG by SW and pinhole defects (Figure 1(e,f)). The simulations are performed using the FE method [20–22].

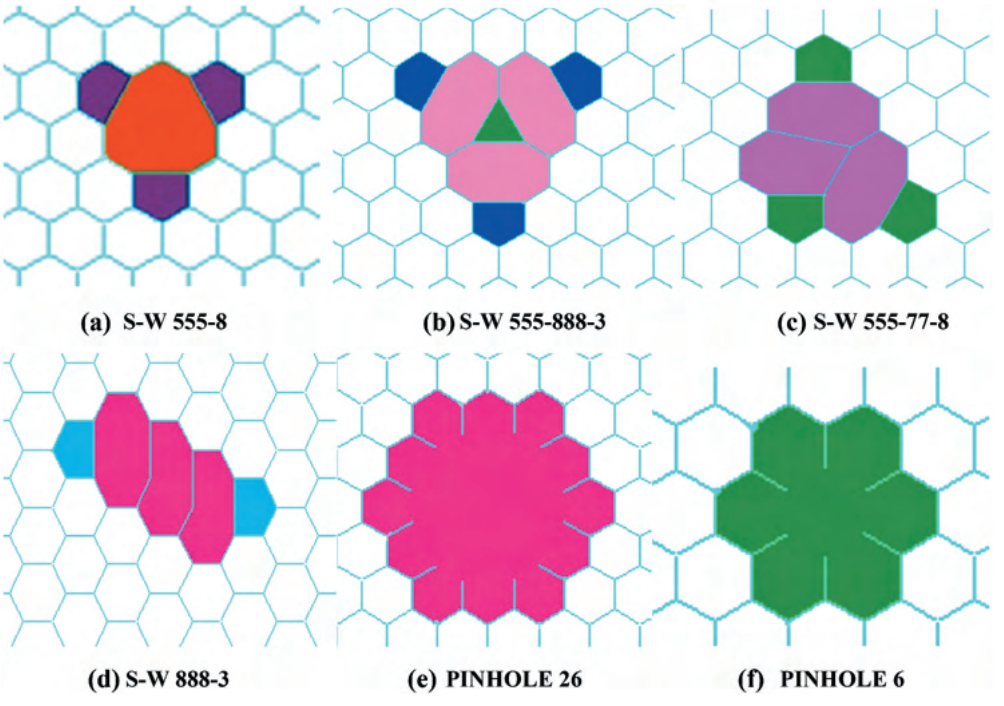

Figure 1. (a) S-W 555-8, (b) S-W 555-888-3, (c) S-W 555-77-8, (d) S-W 888-3, (e) PINHOLE 26 and (f) PINHOLE 6.

2. Methodology

As shown in Figure 2, to model the structure of SLG, elastic beam properties are added to an elastic beam element. The crucial modifications to the graphene lattice are included in the modelling of the pinhole defect throughout the FEM design stages. The elastic modulus and shear modulus of the beam element are, respectively, 1.00 and 0.4 TPa. Density of 2.3 TPa and Poisson's ratio value of 0.3 are considered for evaluation.

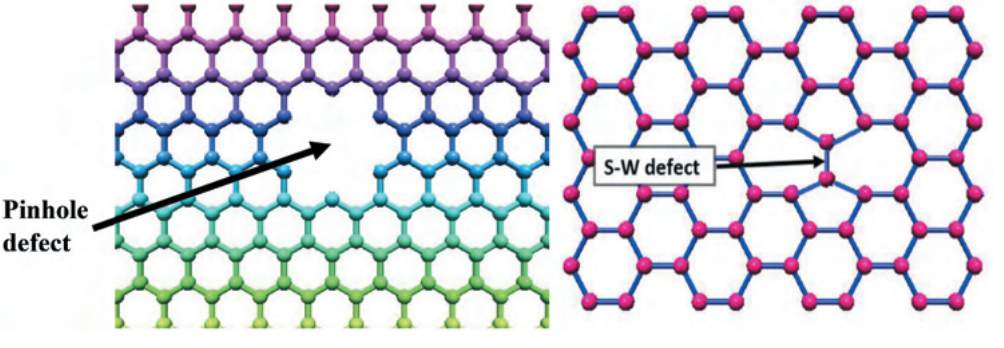

Figure 2. Graphene geometry single-layer graphene with pinhole defect and Stone–Wales defect in the centre of its structure.

This study considers armchair SLG (6 6), (8 8), (10 10); zigzag SLG (12 0), (16 0), (20 0); chiral SLG (16 4); and chiral SLG (12 4). This work investigates the effects of SW and pinhole defects on the zigzag, armchair and chiral SLGs with bridged and cantilever boundary conditions. The C–C bond is represented by a variable cross-section, three-node Timoshenko beam in the proposed enhanced molecular structure. The three-node Timoshenko beam is used to represent the flexibility of the middle C–C bond. For the flexibility of C–C bond, the beam near the joint (short beam) is given a smaller bending stress. Two common instances of in-plane and out-of-plane deformation are used to demonstrate the accuracy of this method as it is used to derive and determine the stiffness matrix of the beam element. The MSM method, which uses point masses and equivalent structural beams, is used to examine the vibrational behaviour of SLGSs. Based on the Odegard approach [23], the elastic characteristics of the beams are calculated by taking the stiffnesses of the covalent bonds into account to simulate the interatomic forces of the connected carbons. The graphene sheet is represented as a space frame structure based on MSM, wherein the bonds between nearby atoms are modelled as beam elements and the atoms are considered as point masses [24–28]. The carbon atoms are viewed as lumped mass elements present at the frame nodes, while the covalent bonds are represented as beams.

2.1. Interatomic FE modeling of SLG

The atomistic model which consists of the beam elements has the capability of simulating covalent interactions of the carbon atoms. Structure of the SLG sheet is created in ANSYS APDL software. In this paper, potential energy is used to analyse linear nano-spring stiffness applying the FE method. The overall force exerted on each atomic nuclei is equal to the sum of the forces exerted by electrons and the electrostatic forces exerted between positively charged nuclei.

$$U = \sum U_r + \sum U_\theta + \sum U_\phi + \sum U_\omega + \sum U_{vdw} \tag{1}$$

where U_{r} is the bond stretch interaction energy, U_{Θ} is the bending energy, U_{Φ} is the dihedral angle torsion energy, U_{w} is the out-of-plane torsion energy and U_{vdw} is the non-bonded Van der Waals' interaction energy.

$$U_r = \frac{1}{2}k_r(r - r_0)^2 = \frac{1}{2}k_r(\Delta \mathrm{r})^2 \tag{2}$$

$$U_\theta = \frac{1}{2}k_\theta(\theta - \theta_0)^2 = \frac{1}{2}k_\theta(\Delta\theta)^2 \tag{3}$$

$$U_\tau = U_\phi + U_\omega = \frac{1}{2}k_\tau(\Delta\phi)^2 \tag{4}$$

where k_{r}, k_{θ} and $k\tau$ are the bond stretching, bond bending and torsional resistance force constants, respectively, while Δr, $\Delta\theta$ and $\Delta\phi$ represent bond stretching increment, bond angle variation and angle variation of bond twisting, respectively.

The second derivatives of the potential energy terms in Equations (2)–(4) with respect to bond length, bond angle and twisting bond angle variations produce the spring stiffness coefficients k_{r}, k_{θ} and $k\tau$ according to Castigliano's theorem. The angle bending

interaction is simulated with an axial nano-spring, using the simplification. The spring stiffness coefficients of Equations (2)–(4) are taken to be equal to = 6.52×10^{-7} N nm^{-1}, $k_\theta = 8.76 \times 10^{-10}$ N nm rad^{-2} and = 2.78×10^{-10} N nm rad^{-2}.

The elements representing the bond are assumed to be elastic beams with Young's modulus E, length L, cross-sectional area A and moment of inertia I.

The strain energy under pure tension N is given by

$$U_A = \frac{1}{2}\int_0^l \frac{N^2}{EA} dl = \frac{1}{2}\frac{N^2 L}{EA} = \frac{EA}{L}(\Delta L)^2 \tag{5}$$

The strain energy of the beam element under pure bending moment M is can be expressed as follows:

$$U_M = \frac{1}{2}\int_0^l \frac{M^2}{EI} dl = \frac{2EI}{L}(\alpha)^2 = \frac{EI}{L}(2\alpha)^2 \tag{6}$$

where α is the rotational angle of beam ends.

Similarly, the strain energy of the beam element under pure twisting moment T is given by

$$U_T = \frac{1}{2}\int_0^l \frac{T^2}{GJ} dl = \frac{1}{2}\frac{T^2 L}{GJ} = \frac{1}{2}\frac{GJ}{L}(\Delta\beta)^2 \tag{7}$$

where J, G and β are the polar moment of inertia, shear modulus and relative rotations of beam ends, respectively.

As the potential energy in the two approaches is independent, energy equivalence of the stored energy of the two approaches, i.e. molecular mechanics and structural mechanics

$$\frac{EA}{L} = K_r \quad \frac{EI}{L} = K_{\theta,} \quad \frac{GJ}{L} = K_\tau \tag{8}$$

The elastic properties of the beam element are given as

$$d = \sqrt{\frac{k_\theta}{k_r}}, \quad E = \frac{k_r^2 L}{4\pi k_\theta}, \; G = \frac{k_r^2 k_\tau^L}{8\pi k_\theta^2} \tag{9}$$

where d, L, E and G represent the diameter, length, Young's modulus and shear modulus of the beam element, respectively.

The stiffness K_s of special spring is defined by following equation [29–32]:

$$K_s = \left(\frac{1}{a_{c-c}\cos(60)^0}\right)^2 k_\theta \tag{10}$$

2.2. Results and discussion

The frequency of a SLG sheet with a bridged boundary condition is shown in Figure 3. The pinhole and SW defects have been created in the structure. For the evaluation, armchair SLG (6 6), (10 10), (8 8); chiral SLG (12 4), (16 4); and zigzag SLG (12 0), (16 0), (20 0) with lengths of 50, 75 and 100 nm were considered. The graphene sheets are represented on the X-axis, and their frequency to various lengths and defects is shown on the Y-axis. Evaluation is carried out

on the SW defects SW (555-8), SW (5-77-5), SW (555-77-8), SW (888-3), and pinhole defects with 24 and 6 missing elements. Graphs show that pinhole defects with six elements missing is having the highest frequency as compared to other defects. Similarly, SW defects show the lowest frequency as compared to pinhole defects. SW (555-8) has minimum frequency as compared to other single-layer sheets. This indicates that SW defects are less significant as compared to pinhole defects. Moreover, from the graph, it is shown that SLG (12 0) at 100 nm length has the lowest frequency and SLG (6 6) at 50 nm length has the highest frequency. This indicates that as the length of the sheet increases, its sensitivity to defects decreases.

The frequency of a SLG sheet with a cantilever boundary condition is shown in Figure 4. A similar type of graphene sheets and defects has been considered for the evaluation. Graphs show that pinhole defect with six elements missing is having the highest frequency as compared to other defects. Similarly, SW defects show the lowest frequency as compared to pinhole defects. SW (555-8) has minimum frequency as compared to other single-layer sheets. This indicates that SW defects are less significant as compared to pinhole defects. Moreover, from the graph SLG (10 10) at 75 nm length has the lowest frequency and SLG (6 6) at 100 nm length has the highest frequency. This indicates when the SLG sheet is fixed at one end (cantilever boundary condition), for 100 nm length of the sheet shows maximum variation in frequency.

Table 1 presents the frequency values for the SLG armchair, zigzag and chiral types. ANSYS APDL software was used to construct a model with pinhole and SW defects. Several models have been created by applying the material properties given in the

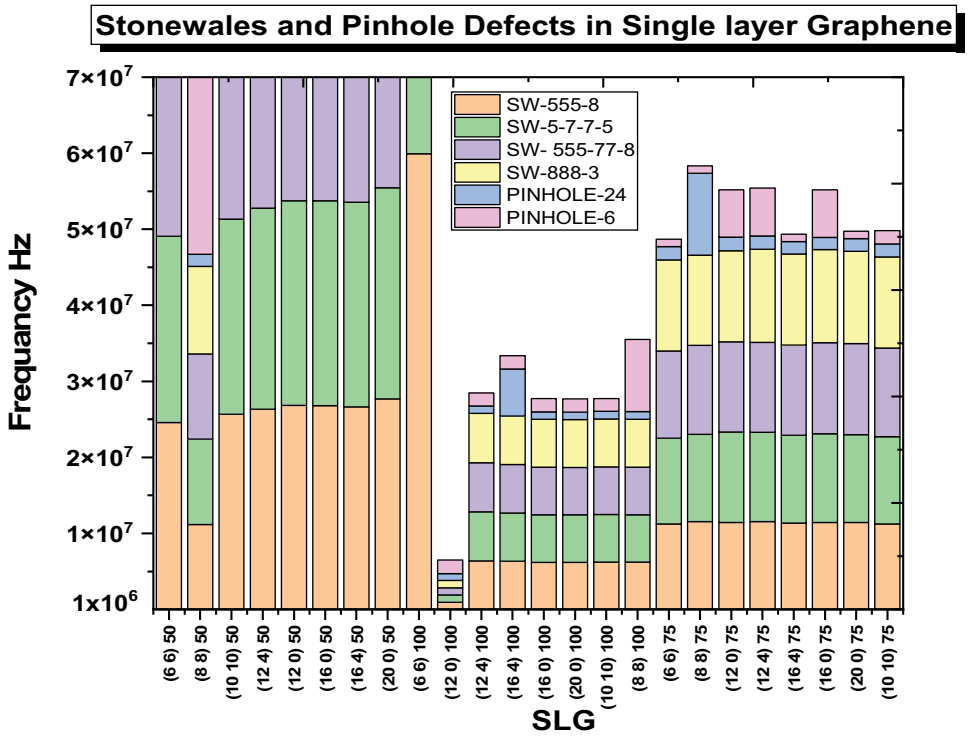

Figure 3. Single-layer graphene Stone–Wales defects vs pinhole defects with bridged condition.

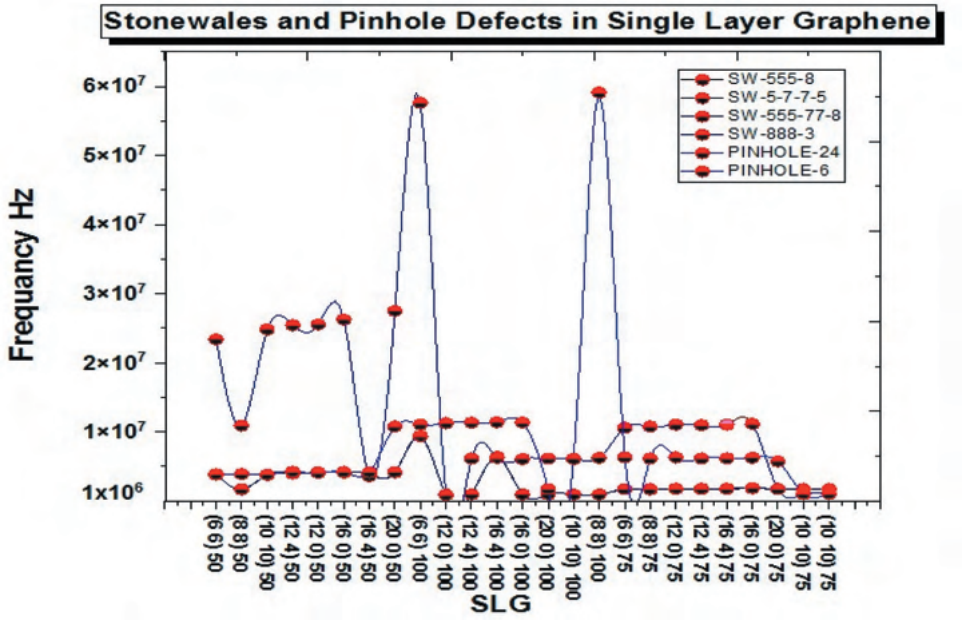

Figure 4. Single-layer graphene Stone–Wales defects vs pinhole defects with cantilever condition .

Table 1. Single-layer graphene (SLG) sheets with pinhole defects and Stone–Wales defects with bridged boundary condition.

	Types of Defects					
Length of Sheet	Stone–Wales (555-8)	Stone–Wales (5-7-7-5)	Stone–Wales (555-77-8)	Stone–Wales (888-3)	Pinhole 24 elements	Pinhole 6 elements
Frequency (Hz)						
50 Nm						
SLG (6 6)	2.46×10^7	2.46×10^7	2.46×10^7	2.46×10^7	2.46×10^7	2.46×10^7
SLG (8 8)	1.12×10^7	1.12×10^7	1.12×10^7	1.15×10^7	1.58×10^6	2.42×10^7
SLG (12 0)	2.46×10^7	2.46×10^7	2.46×10^7	2.46×10^7	2.46×10^7	2.46×10^7
SLG (12 4)	2.46×10^7	2.46×10^7	2.46×10^7	2.46×10^7	2.46×10^7	2.46×10^7
SLG (16 0)	2.46×10^7	2.46×10^7	2.46×10^7	2.46×10^7	2.46×10^7	2.46×10^7
SLG (16 4)	2.46×10^7	2.46×10^7	2.46×10^7	2.46×10^7	2.46×10^7	2.46×10^7
SLG (20 0)	2.46×10^7	2.46×10^7	2.46×10^7	2.46×10^7	2.46×10^7	2.46×10^7
SLG (10 10)	2.46×10^7	2.46×10^7	2.46×10^7	2.46×10^7	2.46×10^7	2.46×10^7
100 Nm						
SLG (6 6)	9.42×10^6	9.36×10^6	9.31×10^6	$9.36E \times 10^6$	8.76×10^6	1.75×10^7
SLG (12 0)	9.59×10^5	9.51×10^5	9.45×10^5	9.55×10^5	9.03×10^5	1.76×10^6
SLG (12 4)	9.67×10^5	9.61×10^5	9.56×10^5	9.64×10^5	9.88×10^5	1.72×10^6
SLG (16 0)	9.58×10^5	9.53×10^5	9.50×10^5	9.55×10^5	6.18×10^6	1.75×10^6
SLG (16 4)	9.62×10^5	9.58×10^5	9.52×10^5	9.57×10^5	9.87×10^5	1.77×10^6
SLG (20 0)	9.56×10^5	9.51×10^5	9.46×10^5	9.54×10^5	9.68×10^5	1.75×10^6
SLG (10 10)	9.58×10^5	9.52×10^5	9.48×10^5	9.53×10^5	9.85×10^5	1.71×10^6
SLG (8 8)	9.62×10^5	9.58×10^5	9.51×10^5	9.56×10^5	9.86×10^5	9.47×10^6
75 Nm						
SLG (6 6)	9.42×10^6	9.36×10^6	9.31×10^6	$9.36E \times 10^6$	8.76×10^6	1.75×10^7
SLG (12 0)	9.59×10^5	9.51×10^5	9.45×10^5	9.55×10^5	9.03×10^5	1.76×10^6
SLG (12 4)	9.67×10^5	9.61×10^5	9.56×10^5	9.64×10^5	9.88×10^5	1.72×10^6
SLG (16 0)	9.58×10^5	9.53×10^5	9.50×10^5	9.55×10^5	6.18×10^6	1.75×10^6
SLG (16 4)	9.62×10^5	9.58×10^5	9.52×10^5	9.57×10^5	9.87×10^5	1.77×10^6
SLG (20 0)	9.56×10^5	9.51×10^5	9.46×10^5	9.54×10^5	9.68×10^5	1.75×10^6
SLG (10 10)	9.58×10^5	9.52×10^5	9.48×10^5	9.53×10^5	9.85×10^5	1.71×10^6
SLG (8 8)	9.62×10^5	9.58×10^5	9.51×10^5	9.56×10^5	9.86×10^5	9.47×10^6

Table 2. Single-layer graphene (SLG) sheets with pinhole defects and Stone–Wales defects with cantilever boundary condition.

	Types of Defects					
Length of Sheet	Stone–Wales (555-8)	Stone–Wales (5-7-7-5)	Stone–Wales (555-77-8)	Stone–Wales (888-3)	Pinhole 24 elements	Pinhole 6 elements
Frequency (Hz)						
50 Nm						
SLG (6 6)	3.83×10^6	3.82×10^6	3.82×10^6	3.82×10^6	2.34×10^7	3.88×10^6
SLG (8 8)	1.69×10^6	1.69×10^6	1.70×10^6	1.72×10^6	1.09×10^7	3.91×10^6
SLG (12 0)	3.78×10^6	3.79×10^6	3.81×10^6	3.82×10^6	2.48×10^7	3.82×10^6
SLG (12 4)	4.02×10^6	4.03×10^6	4.03×10^6	4.05×10^6	2.54×10^7	4.23×10^6
SLG (16 0)	4.15×10^6	4.15×10^6	4.17×10^6	4.18×10^6	2.56×10^7	4.07×10^6
SLG (16 4)	4.14×10^6	4.15×10^6	4.14×10^6	4.16×10^6	2.63×10^7	4.20×10^6
SLG (20 0)	3.87×10^6	3.87×10^6	3.89×10^6	3.92×10^6	3.60×10^6	4.17×10^6
SLG (10 10)	4.14×10^6	4.15×10^6	4.16×10^6	4.19×10^6	2.75×10^7	1.08×10^7
100 Nm						
SLG (6 6)	9.37×10^6	9.37×10^6	9.39×10^6	9.42×10^6	5.76×10^7	1.11×10^7
SLG (12 0)	9.54×10^5	9.55×10^5	9.57×10^5	9.58×10^5	8.58×10^5	1.13×10^7
SLG (12 4)	9.62×10^5	9.64×10^5	9.66×10^5	9.68×10^5	6.16×10^6	1.13×10^7
SLG (16 0)	6.34×10^6	6.36×10^6	6.37×10^6	6.39×10^6	6.23×10^6	1.14×10^7
SLG (16 4)	9.54×10^5	9.56×10^5	9.56×10^5	9.59×10^5	6.09×10^6	1.14×10^7
SLG (20 0)	9.53×10^5	9.54×10^5	9.56×10^5	9.59×10^5	6.16×10^6	1.72×10^6
SLG (10 10)	9.54×10^5	9.55×10^5	9.56×10^5	9.58×10^5	6.12×10^6	6.07×10^6
SLG (8 8)	9.57×10^5	9.59×10^5	9.59×10^5	9.62×10^5	6.25×10^6	5.91×10^7
75 Nm						
SLG (6 6)	1.70×10^6	1.71×10^6	1.72×10^6	1.73×10^6	1.06×10^7	6.33×10^6
SLG (8 8)	1.69×10^6	1.70×10^6	1.71×10^6	1.72×10^6	1.08×10^7	6.16×10^6
SLG (12 0)	1.74×10^6	1.76×10^6	1.77×10^6	1.79×10^6	1.11×10^7	6.30×10^6
SLG (16 0)	1.73×10^6	1.74×10^6	1.75×10^6	1.77×10^6	1.12×10^7	6.17×10^6
SLG (12 4)	1.75×10^6	1.76×10^6	1.77×10^6	1.79×10^6	1.11×10^7	6.19×10^6
SLG (16 4)	1.85×10^6	1.87×10^6	1.89×10^6	1.90×10^6	1.12×10^7	6.25×10^6
SLG (20 0)	1.74×10^6	1.74×10^6	1.74×10^6	1.74×10^6	1.75×10^6	5.75×10^6
SLG (8 8)	1.69×10^6	1.70×10^6	1.71×10^6	1.72×10^6	1.01×10^6	1.06×10^6

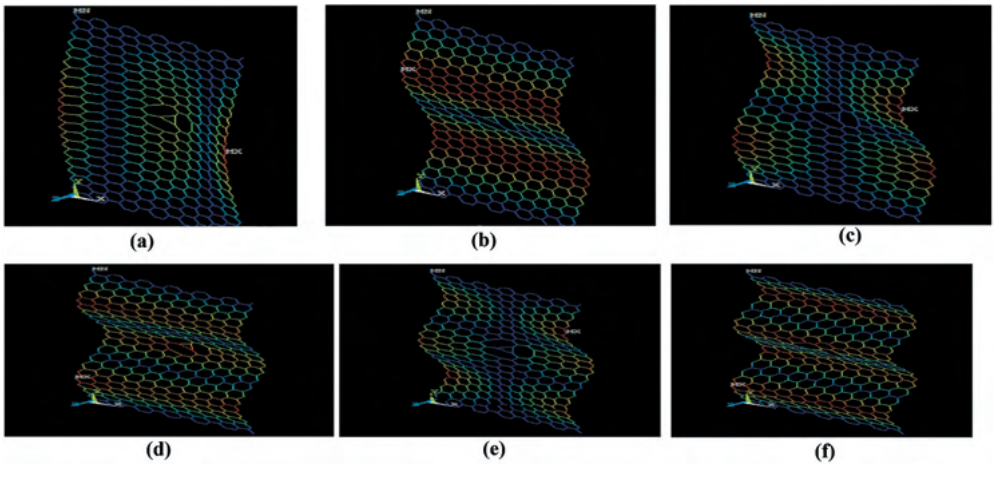

Figure 5. (a–f) Mode shapes of SLG armchair (6 6) with Stone–Wales defect (555-888-3).

introduction part of the material modelling section. Pinhole and SW defects were produced by applying bridged boundary conditions at the ends of the graphene lattice. It even shows the frequency attained with length variation. Results from graphene

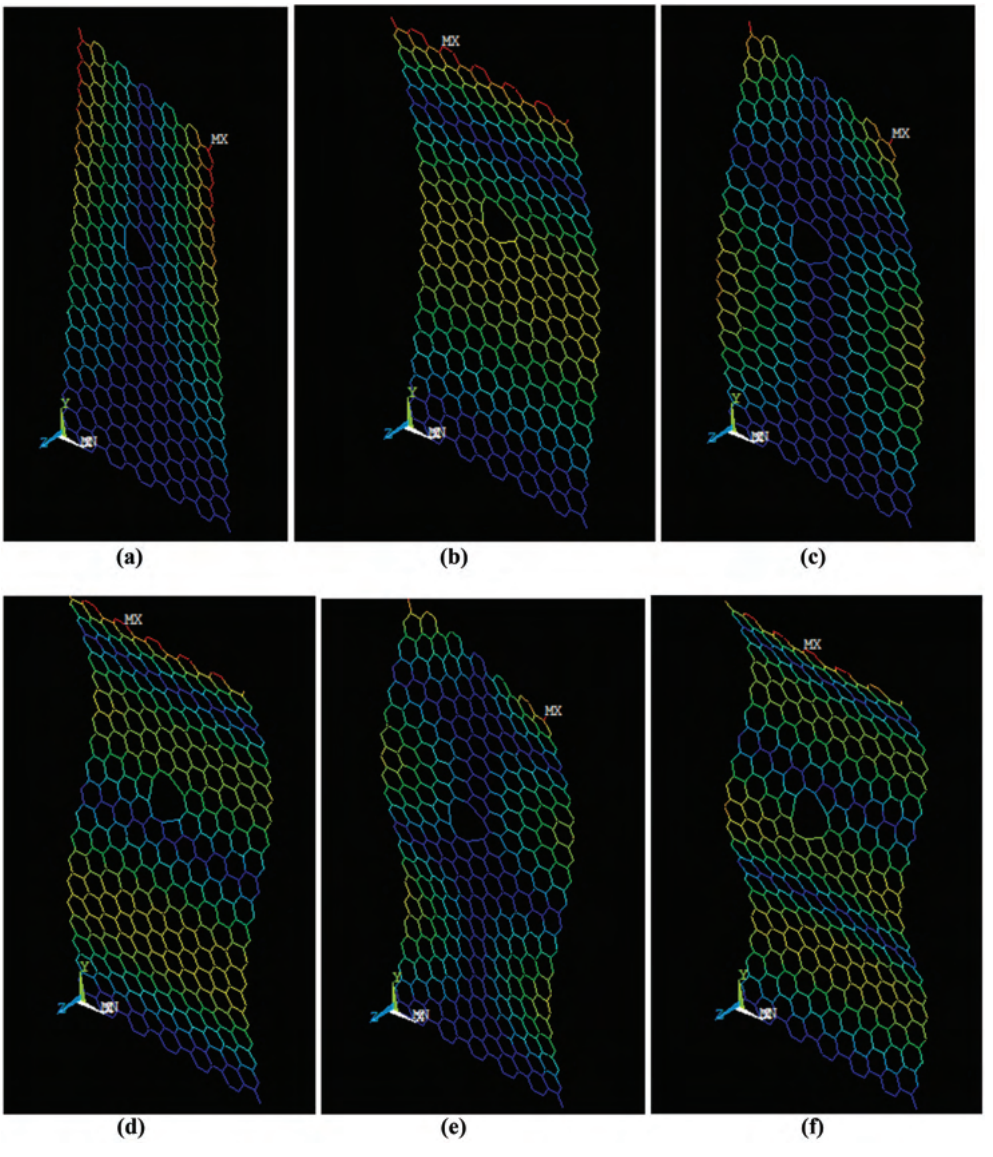

Figure 6. (a–f) Mode shapes of SLG armchair (6 6) with Stone–Wales defect (555-8).

modelling with a cantilever boundary condition are shown in Table 2. Frequency values vary when different boundary conditions were applied to the graphene structure. It shows that when the structure's conditions change, the results also change. According to the table, pinhole defects play a significant role in the dynamic behaviour of SLG.

The vibrational behaviour of SLG sheets has been examined using a MSM approach. Mode shapes and natural frequencies are obtained by using this method. The position of the defect is at the centre of the 50-nm graphene sheet. The analysis of vibrations is carried out under bridged boundary conditions. As shown in Figure 5 (a–f) the variation in mode shapes of the graphene sheet is fixed at both ends. It

shows a behavioural change in the shape and frequency of the SLG sheet armchair (6 6) of length 50 Nm. A similar kind of configuration is considered for analysis under cantilever conditions. Figure 6(a-f) shows the mode shapes of SLG with cantilever boundary conditions. SW (555-8) defect is created at the centre of the graphene sheet. The vibrational behaviour of graphene changes after the second mode shape. It shows the effect of the defect on the graphene structure which is a very useful analysis for graphene-based sensors.

3. Conclusion

This study examines how nanoscale defects affect the behaviour of graphene sheets. In this case, FEM computation methods are implemented to examine the effects of defects on chiral-, zigzag- and armchair-oriented graphene. The effect of defects such as pinhole and SW on the resonance frequency in chiral, zigzag and armchair SLG is investigated using an atomistic molecular dynamic analysis. The study considers armchair SLG (6 6), (8 8), (10 10); zigzag SLG (12 0), (16 0), (20 0), chiral SLG (16 4); and SLG (12 4). A common graphene symmetry reconfiguration produces three pentagons and one octagon (555-8) (Figure 1(a)). The absence of carbon atoms causes another defect in the lattice structure (555-888-3) (Figure 1(b)). One bond resulted in the defects (888-3) and (555-77-8), shown in Figure 1(c,d), respectively. As shown in Figure 1(e,f), pinhole defects are caused by 6 missing carbon atoms and 26 missing carbon atoms. The following conclusion is drawn from the analysis.

(1) With the increase in the length of the graphene sheet, the effect of SW defect decreases.
(2) Pinhole defects show more variation in frequency as compared to SW defects.
(3) Large graphene sheet shows less sensitivity towards defects.
(4) Lower dimensions show more frequency reduction in pinhole defects as more elements have been removed as compared to larger dimensions.
(5) The boundary condition of the FE analysis also affects the vibrational behaviour of the graphene sheets.

It shows that the effect of defect does not depend only on the size and chirality of graphene. These results are useful for defective SLG-based nanosensors. This work clarifies how defective graphene can be used for multipurpose applications and for technical design in manufacturing processes.

Disclosure statement

No potential conflict of interest was reported by the authors.

Future scope

Rarely does one get an ideal flat graphene membrane with defectless characteristics. The real condition of view differs significantly from the theoretically expected graphene qualities. In fact, 2D graphene membranes have a propensity to crack, produce bubbles and ripples,

reorganise and produce various defects. Graphene has a wide range of possible applications and has grown significantly in recent years. Producing and working with graphene is still difficult, as is regulated, industrial-scale production of high-quality graphene. More applications in the field of nano-resonators will be made possible by further research into defective graphene.

References

[1] Roco MC, Mirkin CA, Hersam MC. Nanotechnology research directions for societal needs in 2020: retrospective and outlook. Vol. 1. Springer Science & Business Media; 2011.
[2] Zandiatashbar A, Lee GH, An SJ, et al. Effect of defects on the intrinsic strength and stiffness of graphene. Nat Commun. 2014;5(1):1–9.
[3] Plimpton S. Fast parallel algorithms for short-range molecular dynamics. J Comput Phys. 1995;117(1):1–19.
[4] Novoselov KS, Geim AK, Morozov SV, et al. Electric field effect in atomically thin carbon films. Science. 2004;306(5696):666–669.
[5] Geim AK. Graphene: status and prospects. Science. 2009;324(5934):1530–1534.
[6] Geim AK. Nobel Lecture: random walk to graphene. Rev Mod Phys. 2011;83(3):851.
[7] Novoselov KS. Nobel lecture: graphene: materials in the flatland. Rev Mod Phys. 2011;83 (3):837.
[8] Wei D, Liu Y. Controllable synthesis of graphene and its applications. Adv Mater. 2010;22 (30):3225–3241.
[9] Banhart F, Kotakoski J, Krasheninnikov AV. Structural defects in graphene. ACS Nano. 2011;5(1):26–41.
[10] Rodríguez-Pérez L, Herranz MÁ, Martín N. The chemistry of pristine graphene. Chem Comm. 2013;49(36):3721–3735.
[11] Gao X, Wang Y, Liu X, et al. Regioselectivity control of graphene functionalization by ripples. Phys Chem Chem Phys. 2011;13(43):19449–19453.
[12] Lu J, Bao Y, Su CL, et al. Properties of strained structures and topological defects in graphene. ACS Nano. 2013;7(10):8350–8357.
[13] Zsoldos I. Effect of topological defects on graphene geometry and stability. Nanotechnol Sci Appl. 2010;3:101.
[14] Araujo PT, Terrones M, Dresselhaus MS. Defects and impurities in graphene-like materials. Mater Today. 2012;15(3):98–109.
[15] Skoda M, Dudek I, Jarosz A, et al. Graphene: one material, many possibilities—application difficulties in biological systems. J Nanomater. 2014;2014:1–11.
[16] Patel Ajay M, Joshi AY. Vibration analysis of double wall carbon nanotube based resonators for zeptogram level mass recognition. Comput Mater Sci Elsevier Publishers. 2013;79:230–238.
[17] Patel Ajay M, Joshi AY. Investigating the influence of surface deviations in double wall carbon nanotube based nanomechanical sensors. Comput Mater Sci. 2014 April;89:157–164.
[18] Patel AM, Joshi AY. Effect of waviness on the dynamic characteristics of double walled carbon nanotubes. Nanosci Nanotechnol Lett. 2014;6:1–9.
[19] Patel AM, Joshi AY. Influence of atomic vacancies on the dynamic characteristics of nano resonators based on double walled carbon nanotube. Physica E. 2015;70(c):90–100.
[20] Makwana M, Patel AM, Oza AD, et al. Effect of mass on the dynamic characteristics of single-and double-layered graphene-based nano resonators. Materials. 2022;15(16):5551.
[21] Makwana MV, Patel AM. Molecular dynamic analysis of pristine single layered graphene for mass sensor. Materials Today: Proceedings. 2022;72(2023):729–735.
[22] Makwana MV, Patel AM. Recent applications and synthesis techniques of graphene. Micro Nanosyst. 2022;14(4):287–303.
[23] Sakhaee-Pour A, Ahmadian MT, Naghdabadi R. Vibrational analysis of single-layered graphene sheets. Nanotechnology. 2008;19(8):085702.

[24] Li C, Chou TW. A structural mechanics approach for the analysis of carbon nanotubes. Int J Solids Struct. 2003;40(10):2487–2499.
[25] Wang CG, Xia ZM, Tan HF. An improved molecular structure mechanics method and its application for graphene wrinkling. Int J Eng Sci. 2016;106:168–178.
[26] Zhao P, Shi G. Study of Poisson's ratios of graphene and single-walled carbon nanotubes based on an improved molecular structural mechanics model. Struct Longv. 2011;5 (1):49–58.
[27] Hashemnia K, Farid M, Vatankhah R. Vibrational analysis of carbon nanotubes and graphene sheets using molecular structural mechanics approach. Comput Mater Sci. 2009;47(1):79–85.
[28] Firouz-Abadi RD, Moshrefzadeh-Sany H, Mohammadkhani H, et al. A modified molecular structural mechanics model for the buckling analysis of single layer graphene sheet. Solid State Commun. 2016;225:12–16.
[29] Georgantzinos SK, Katsareas DE, Anifantis NK. Limit load analysis of graphene with pinhole defects: a nonlinear structural mechanics approach. Int J Mech Sci. 2012;55 (1):85–94.
[30] Chakraborty D, Rathi A, Singh A, et al. Determination of mechanical properties of graphene reinforced Tetra-GEDVA nanocomposite. Mater Phys Mech. 2020;44(3):324–331.
[31] Ali SJ, Goyal A, Dadhich M, et al. Design optimization of prosthesis hip joint using fem and design of experiment approach. Biomed Eng Appl Basis Commun. 2020;32(06):2050048.
[32] Goyal A, Kothari B, Pathak VK. Fuzzy logic and desirability-based models for predicting performance characteristics of varying concentration graphite nanoplatelets (GNPs) mixed nanofluid MQL in turning of AISI-1045 steel. Int J Interact Des Manuf (IJIDeM). 2022;16 (4):1559–1584.